ACS central science

Research Article

http://pubs.acs.org/journal/acscii

The Impact of Aerosol Particle Mixing State on the Hygroscopicity of Sea Spray Aerosol

Steven R. Schill,[†] Douglas B. Collins,[†] Christopher Lee,[†] Holly S. Morris,[‡] Gordon A. Novak,[§] Kimberly A. Prather,[†,∥] Patricia K. Quinn,[⊥] Camille M. Sultana,[†] Alexei V. Tivanski,[‡] Kathryn Zimmermann,[†] Christopher D. Cappa,[#] and Timothy H. Bertram*[,§]

[†]Department of Chemistry and Biochemistry, University of California San Diego, La Jolla, California 92093, United States

[‡]Department of Chemistry, University of Iowa, Iowa City, Iowa 52242, United States

[§]Department of Chemistry, University of Wisconsin Madison, Madison, Wisconsin 53706, United States

[∥]Scripps Institution of Oceanography, La Jolla, California 92037, United States

[⊥]Pacific Marine Environmental Laboratory, National Oceanic and Atmospheric Administration, Seattle, Washington 98115, United States

[#]Department of Civil and Environmental Engineering, University of California Davis, Davis, California 95616, United States

Supporting Information

ABSTRACT: Aerosol particles influence global climate by determining cloud droplet number concentrations, brightness, and lifetime. Primary aerosol particles, such as those produced from breaking waves in the ocean, display large particle−particle variability in chemical composition, morphology, and physical phase state, all of which affect the ability of individual particles to accommodate water and grow into cloud droplets. Despite such diversity in molecular composition, there is a paucity of methods available to assess how particle−particle variability in chemistry translates to corresponding differences in aerosol hygroscopicity. Here, an approach has been developed that allows for characterization of the distribution of aerosol hygroscopicity within a chemically complex population of atmospheric particles. This methodology, when applied to the interpretation of nascent sea spray aerosol, provides a quantitative framework for connecting results obtained using molecular mimics generated in the laboratory with chemically complex ambient aerosol. We show that nascent sea spray aerosol, generated in situ in the Atlantic Ocean, displays a broad distribution of particle hygroscopicities, indicative of a correspondingly broad distribution of particle chemical compositions. Molecular mimics of sea spray aerosol organic material were used in the laboratory to assess the volume fractions and molecular functionality required to suppress sea spray aerosol hygroscopicity to the extent indicated by field observations. We show that proper accounting for the distribution and diversity in particle hygroscopicity and composition are important to the assessment of particle impacts on clouds and global climate.

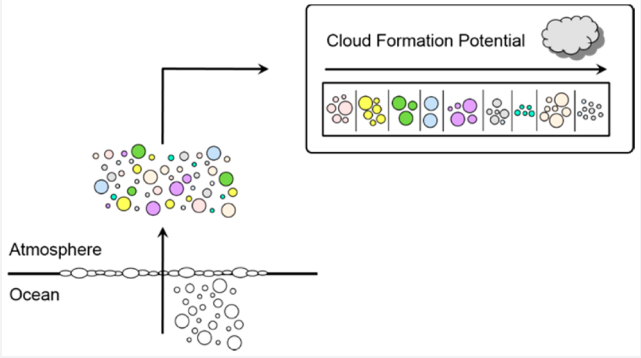

1. INTRODUCTION

Atmospheric aerosol particles impact global climate directly through interactions with incoming solar radiation and indirectly by seeding the formation and controlling the properties of all cloud droplets, which alters Earth's radiation budget.[1] The ability of a particle to take up water from its surrounding environment and act as a cloud seed, or cloud condensation nucleus (CCN), is intimately linked to particle chemical composition, especially for particles with dry diameters less than 200 nm.[2] Measurements of the molecular composition of individual aerosol particles in this size regime are rare,[3] thus limiting our ability to connect heterogeneity in particle chemical composition with their ability to serve as CCN at a single particle level. Here, we present a new methodology for direct characterization of the distribution of aerosol hygroscopicity as driven by particle−particle compositional variability within a complex population of atmospheric particles. We demonstrate that this approach, when applied to nascent sea spray aerosol (SSA), permits unique perspective on the influence that particle chemical diversity plays in determining the impacts of particles on climate. Further, we show that the generality of the approach permits quantitative comparison between laboratory−generated molecular mimics and actual nascent SSA generated in situ in the Atlantic Ocean.

Received: April 25, 2015
Published: June 9, 2015

DOI: 10.1021/acscentsci.5b00174
ACS Cent. Sci. 2015, 1, 132−141

The hygroscopicity of an individual particle is a function of its chemical composition with, in general, inorganic salts leading to a more hygroscopic particle and organic materials leading to a less hygroscopic particle.[4] Hygroscopicity displays further variability within the organic and inorganic component classes, dependent upon factors such as solubility, molecular weight, and surface tension. The hygroscopicity of particles can be characterized through measurements of their ability to activate into droplets or activation efficiency, i.e., the fraction of particles of a given size that grow into droplets when exposed to a given water supersaturation (s), or $f_{CCN}(s)$; the more hygroscopic a particle, the larger the activation efficiency. Such determinations are referred to as size-resolved CCN (SR-CCN) measurements. The activation efficiency for particles of fixed composition is also size-dependent, with larger particles having a larger $f_{CCN}(s)$ at a given s. Therefore, particle hygroscopicity is routinely quantitatively characterized by converting direct measurements of a selected particle diameter (D_p) and the critical supersaturation (s_{crit}, where 50% of the particle population has activated) to a single parameter, κ;[5] smaller κ-values correspond to less hygroscopic particles and vice versa. The so-called κ-Köhler theory separates the intrinsic hygroscopicity (composition dependence) from the particle size dependence, thereby allowing for assessment of the influence of composition more specifically. Typical values of κ range between 0 and 1.4, with lower values generally associated with less soluble (or insoluble) organic compounds, and higher values generally associated with soluble inorganic compounds.[5,6] For SSA particles, composition is dictated both by the chemistry and biology that occurs in the ocean to produce a wide variety of organic compounds, especially near the sea surface, and by the transfer of those compounds to SSA.[7,8] Size-resolved particle composition measurements have demonstrated that the organic fraction increases as particle size decreases, when considered either by mass[9−11] or by number.[12,13] The hygroscopicity of SSA in the submicrometer size regime has been previously found to vary with size, especially for particles with diameters below 100 nm, which has been interpreted as indicating enrichment of organic material in smaller particles.[2,14,15]

On top of such general enrichment in SSA organic content with decreasing particle size, individual nascent SSA particles also display a wide diversity of individual particle types.[12,13,16−19] These different particle types have distinct compositions with respect to the relative abundance and chemical nature of the organic material. Such mixing-state effects will influence the actual overall activation behavior of a distribution of particles, as always exists in the ambient atmosphere and in some laboratory experiments. Despite this complexity, typical analyses of ambient particle CCN activation assume that all particles of a given size have identical composition (i.e., are internally mixed) and therefore report effective κ-values that may, or may not, fully describe the actual impacts of the distribution. As just a few examples, effective κ-values have been reported for pristine aerosols in the Amazonian rainforest,[20] aged aerosols in the highly polluted Chinese city of Guangzhou,[21] and nascent marine SSA from the WACS I cruise in the Atlantic Ocean.[14] Importantly, global models have suggested that aerosol mixing state can impact CCN concentrations by up to 20% in the case of marine SSA,[22,23] indicating that improved constraints on aerosol mixing state and how this varies by source are still necessary for robust determination of CCN concentrations.

Direct measurements of CCN concentrations are often compared to volume-mixing based predictions from Köhler theory, where incorporation of size-dependent chemical composition results in model-measurement agreement to within 10−20%,[24−30] but these still do not deal with the inherent particle−particle compositional variability at a given size. Padró et al.[31] found that accounting for external mixing improved CCN number concentration predictions (within 10−20% of measured), while the common internal mixing state assumption can have a significantly greater error associated with it (up to 100%), in agreement with prior studies focused on externally mixed aerosols.[24,25]

Of specific relevance to this work, Collins et al.[32] investigated the CCN activity of SSA generated from a large-scale mesocosm seawater experiment and found that the assumption that all particles were compositionally identical (internally mixed) was insufficient to explain the temporal changes in the SSA particle hygroscopicity. Instead, a model in which the SSA was assumed to contain a diversity of particles with distinct compositions (externally mixed) was needed.[32] The apparent need for robust methods that can account for mixing state in the interpretation of CCN measurements is supported by measurements of particle growth due to water uptake under subsaturated conditions, which often indicate the coexistence of particles with very different compositions and hygroscopicities.[33,34] Despite the evident need for CCN-specific hygroscopicity analyses that routinely account for the actual diversity of particles, few CCN studies have considered implementing a distribution of hygroscopicity values, or how a distribution of hygroscopicity values may be detected using SR-CCN measurements.[35,36]

In what follows, we develop a quantitative framework for assessing the distribution of aerosol hygroscopicity for populations of sub-100 nm aerosol particles. The methodology bridges molecular mimics of increasing complexity, from single-component particles to internally and externally mixed heterogeneous populations, with nascent SSA particles generated from synthetic and microcosm phytoplankton bloom experiments and from the ambient surface ocean waters. Implications of this methodology for understanding chemical diversity and climate impacts of SSA particles specifically, and atmospheric aerosol particles in general, are discussed.

2. INFLUENCE OF MIXING STATE ON CCN ACTIVITY

In this section, a bottom-up approach is used to facilitate the development of a quantitative methodology to assess the influence of particle mixing state on CCN activity, starting with chemically simple (single-component) systems and systematically increasing the system complexity with respect to the particle−particle chemical diversity. The hygroscopicities of internal and external particle mixtures of known composition have been characterized through measurement of CCN activation curves (Methods; Figure S1). The compounds studied here were selected based on the consideration of the evolution of surface seawater chemical composition throughout the successive stages of an ocean phytoplankton bloom.[37−39] These SSA organic compound mimics included a refractory hydrocarbon material (cholesterol), a sugar (galactose), a lipopolysaccharide (LPS, from *Escherichia coli* 0111:B4), a protein (bovine serum albumin), and a fatty acid (DPPA, dipalmitoyl phosphatidic acid) (Table 1). The pure organic SSA mimics were considered either individually or as mixtures with synthetic sea salt, which is composed of inorganic ions in

DOI: 10.1021/acscentsci.5b00174
ACS Cent. Sci. 2015, 1, 132−141

Table 1. Literature Solubilities[46] and Measured κ-Values for Single-Component, Pure Sea Spray Aerosol Model Compounds

compound	solubility (g/L)	κ
sea salt	360[a]	0.800−1.106[b]
cholesterol	5×10^{-3}	n/a
galactose	683	0.198 ± 0.028
LPS	5	0.038 ± 0.004
albumin	40	0.031 ± 0.002
DPPA	<1	0.297 ± 0.039

[a]The solubility of synthetic sea salt was assumed to be equivalent to that of sodium chloride. [b]The κ-value for synthetic sea salt was found to vary from lot to lot. The reported κ-values indicate the range of obtained values.

representative seawater concentrations. Model external mixtures were generated by multiple atomizers or nebulizers operating in parallel (Methods).

2.1. Single-Component SSA Mimics. κ-Values were experimentally determined for the five pure organic SSA mimics and for synthetic sea salt from measurement of their activation curves (Table 1). These marine-focused measurements expand the database of compounds for which κ-values have been determined in the laboratory, which includes inorganic salts[5] and slightly soluble organics[40−42] that had generally been chosen based on their relevance to terrestrially derived organics. It was not possible to determine κ-values for cholesterol specifically due to its poor solubility in water. Variability in the measured κ-values for the synthetic sea salt was observed between multiple lots as indicated by the range in values presented in Table 1. The κ-values measured for the organic compounds do not correlate directly with solubility (Table 1). The largest κ-value was observed for DPPA, which has the lowest solubility (excluding cholesterol), which we hypothesize is due in part to formation of vesicle structures by DPPA (critical micelle concentration = 0.46 nM) in an aqueous matrix. Despite its high solubility the κ-value for galactose was lower than DPPA, possibly due to the initially dry galactose particles existing in a highly viscous, glassy state that can impede water uptake.[43] Further, deviations between measured and predicted κ-values (based on solubility alone) may reflect differences in droplet surface tension due to surface partitioning.[44,45] The smallest κ-values were measured for LPS and albumin, which were of intermediate relative solubility.

2.2. Internally Mixed SSA Mimics. Experimental κ-values were determined for two-component internal mixtures of synthetic sea salt (κ = 1.106 for the specific lot used in this experiment) and galactose (κ = 0.198) of varying relative composition (Figure 1). The κ-value of an internal mixture ($\kappa_{mix,int}$) is commonly estimated from volume-mixing rules, where $\kappa_{mix,int} = \sum \varepsilon_i \kappa_i$ and ε_i is the volume fraction of each compound.[5] For a two-component mixture the predicted $\kappa_{mix,int}$ varies linearly with ε_{org} (in this case, $\varepsilon_{galactose}$) and is dependent on the κ-value of the pure compounds. The observed and predicted κ-values for the sea salt:galactose mixtures agreed to within 20% (Figure 1), consistent with previous laboratory observations for other mixtures.[5]

Field determinations of effective κ-values for nascent SSA[14] with dry diameters of 40−100 nm range between 0.4 and 0.9, which corresponds to ε_{org} between ca. 80% and 25% based on the sea salt:galactose mixture results (Figure 1). Because the density of sea salt is similar to that of galactose, this

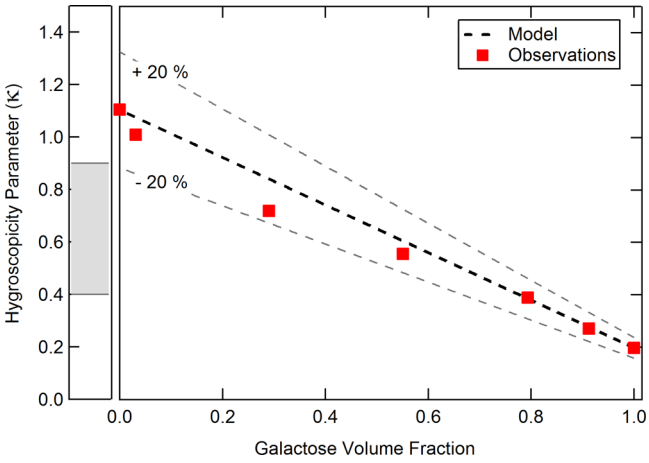

Figure 1. Predicted κ hygroscopicity parameter values for internally mixed, two-component particles of sea salt:galactose as a function of the organic volume fraction (black dashed line), compared with measured κ-values for several sea salt:galactose ratios (red squares). The gray bar on the left shows the range of effective κ-values observed for primary nascent SSA in the marine boundary layer.[14]

corresponds to a mass fraction of approximately the same value. Variability in the actual density of ocean organics can complicate the volume to mass fraction conversion relationship. Previous studies suggest that total and/or water-insoluble organic mass fractions for marine SSA are on the order of 80% for sub-100 nm particles,[10,11] though only around 25% of this mass is water-soluble organics such as galactose.[9] With regard to CCN, distinguishing between the contributions of water-soluble versus water-insoluble organics can additionally be important in obtaining closure.[47] These findings provide context for the validity of an 80% organic particle and how that may affect SSA hygroscopicity, though additional work needs to be done to better characterize the solubility effects of SSA organics, especially in light of the results for DPPA.

2.3. Externally Mixed SSA Mimics. The major existing framework for both measuring supersaturated aerosol hygroscopicity and interpreting the observations relies on the assumption that particles of a given size are internally mixed. However, field studies[48] and laboratory investigations[12,13] have shown that the ensemble of nascent SSA particles is not internally mixed, but instead individual particles exhibit a wide range of per-particle organic volume fractions and organic types. Further, the observed variability and absolute values of effective κ-values for nascent SSA particles that were produced during a large scale mesocosm experiment has been interpreted as indicating that explicit accounting of the particle mixing state in framework for interpreting CCN measurements is needed.[32] One such framework was proposed by Su et al.,[36] who calculated cumulative distribution functions from CCN activation curves, which can be deconstructed into cumulative hygroscopicity distributions. Here, we expand on this framework and provide the explicit validation that has thus far been missing.

A necessary first step in assessing the extent to which CCN activation curves can be used to resolve aerosol mixing state is to characterize the behavior of known external mixtures using high-resolution SR-CCN measurements. It is commonly assumed that activation curves can be fit using a Boltzmann sigmoidal. The activation curve for a single particle type is associated with a characteristic sigmoid slope, or width in f_{CCN}

DOI: 10.1021/acscentsci.5b00174
ACS Cent. Sci. 2015, 1, 132−141

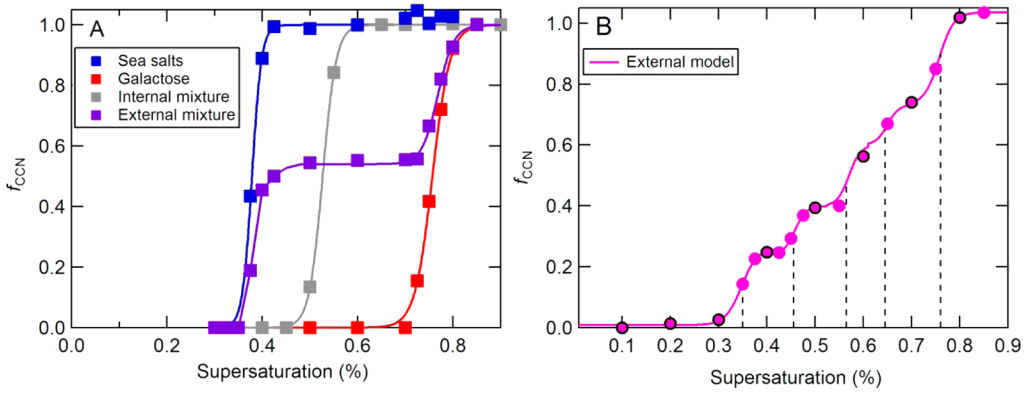

Figure 2. (A) CCN activation curves for 50 nm size selected particles of sea salt (blue), galactose (red), and an internal and external mixture of 1:1 sea salt:galactose (gray and purple respectively). (B) CCN activation curve for 50 nm size selected particles from an external mixture of five particle types: (i) sea salt particles; (ii) a 43:57 by mass sea salt:galactose mixture; (iii) a 22:78 sea salt:galactose mixture; (iv) a 9:91, sea salt:galactose mixture; and (v) pure galactose particles. The points with black circles indicate the points that would have been measured in an SR-CCN experiment at typically used resolution, while the pink points are the actual higher resolution data collected here. The vertical dashed lines show the theoretical s_{crit} for each particle type in the external mixture.

versus s, that is set by the transfer function of the DMA (Figure S2) and the distribution in s in the SR-CCN. Here, the average slope of the sigmoidal fits for all of the pure compounds studied was 0.0180 ± 0.0095 for κ-values between 0.031 and 1.106, demonstrating uniform hygroscopicity among the particle population. Since the inherent methodologically determined slope is very small, in theory the activation of the individual subpopulations of particle types within the overall distribution should be observable if the scanning resolution is sufficiently high. Here, this is examined explicitly by measuring activation curves for external mixtures of particles with known, but differing, composition.

As a first test, activation curves were measured for pure sea salt particles, pure galactose particles, a 1:1 internal mixture of sea salt:galactose particles, and a 1:1 external mixture (Figure 2A). A small fraction (usually <10%) of the aerosol population is doubly charged post−size selection, and is observed as a plateau of activated particles at a lower s value with a sigmoid height much smaller than that of the majority singly charged population. This experimental artifact has been accounted for following the approach of Rose et al.[49] whereby the doubly and singly charged populations are treated as distinct. The resulting normalized activation curves for this study, such as those in Figure 2A, are for the singly charged particles in the population. The activation curve for the external mixture is characterized by two clearly distinguishable sigmoids, which is distinct from the pure compounds and the 1:1 internal mixture, which are all characterized by a single sigmoid. This result highlights the capability of measurements at high s resolution to distinguish aerosol mixing state for subpopulations of particles that have different κ-values. In this example the fraction of particles that activated at the s_{crit} for galactose (0.740% s) was 0.45, and the fraction of particles that activated at the s_{crit} for this sea salt lot (0.378% s) was 0.55, well within the uncertainty of the experimental number fractions. This demonstrates that the sigmoid analysis of high resolution SR-CCN measurements can be used to quantitatively determine the relative concentrations of the externally mixed particle types and that the number of sigmoids corresponds to the number of particle types (with respect to hygroscopicity) while the magnitude of each sigmoid corresponds to the relative abundance of each type.

The two-component system above has been expanded upon by measuring the activation curve for an externally mixed system with five distinct particle types, ranging from pure sea salt to pure organic. By systematically increasing the chemical complexity of the system it is possible to assess the extent to which high s resolution SR-CCN measurements can provide quantitative information on the distribution of κ-values in a given particle population. The particle types considered were internal mixtures with sea salt:galactose mass ratios of 100:0, 43:57, 22:78, 9:91, and 0:100 with corresponding $\kappa_{int,mix}$ values of 0.83, 0.48, 0.34, 0.26, and 0.2, respectively. The relative number concentrations of the different particle types were 0.2, 0.12, 0.28, 0.10, and 0.3. If all of the particle types were mixed together in these proportions, the overall $\kappa_{int,mix}$ = 0.40 ($s_{crit,50nm}$ = 0.52%). A key observation is that clear steps are evident in the activation curve that correspond to the activation of the individual particle types (Figure 2B). This demonstrates that it is possible to resolve the individual particle types within a chemically complex mixture in the activation curve when fine enough steps are taken in s. However, the overall activation curve has a slope that is approximately eight times broader than that of any pure compound or internal mixture when fit with a single sigmoid (Figure 2B). This indicates that broadening of the activation curve occurs for an external mixture of particles that have a range of κ-values, generally consistent with the ambient observations.[7,21,35] It also demonstrates that, with increasing chemical complexity, it is increasingly difficult to fit a distinct number of sigmoids to determine the number of distinct particle types, as the activation curve becomes a broad continuum of activation for multiple populations. A second important observation is that the effective κ that is determined from the observed s_{crit} ($s_{crit,obs}$ = 0.58%) is smaller than that predicted from internal mixing of all the particle types in their known proportions. Specifically, the effective κ_{obs} = 0.32 whereas the predicted $\kappa_{int,mix}$ = 0.40 (corresponding to $s_{crit,50nm}$ = 0.52%).

Using this well-constrained, yet complex (five-component) model system as a test bed, a model framework for fitting the multicomponent activation curve has been developed in which the overall activation curve is quantitatively considered in terms of the contributions from the individual components. Specifically, the five-component external mixture activation

DOI: 10.1021/acscentsci.5b00174
ACS Cent. Sci. 2015, 1, 132−141

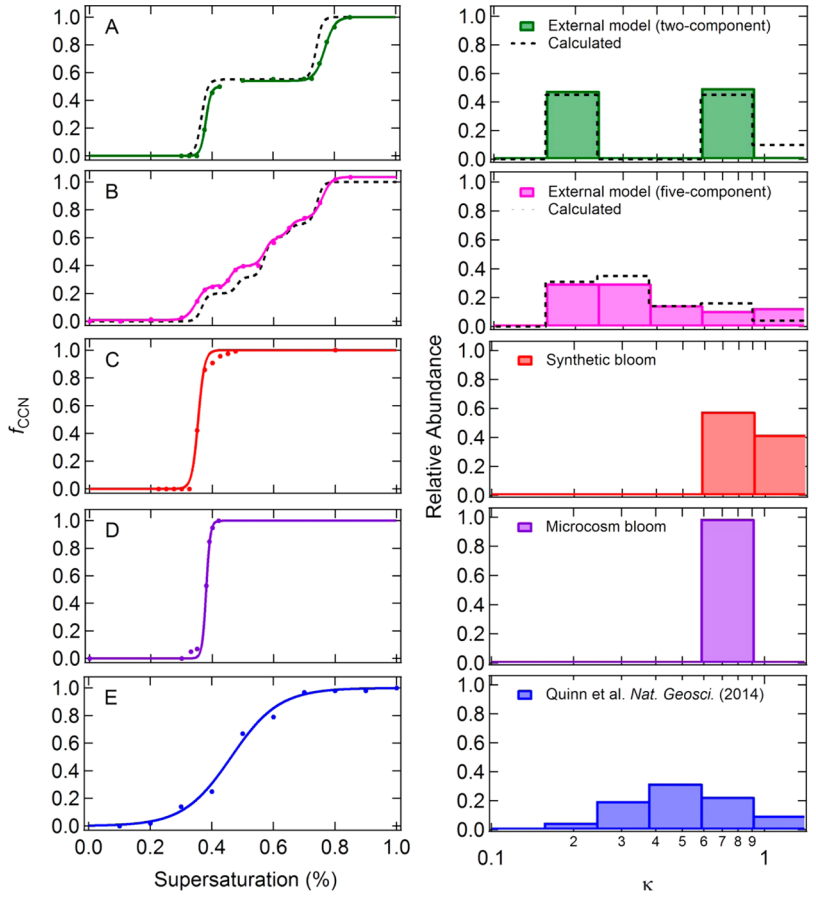

Figure 3. (Left) SR-CCN activation curves and (right) κ distributions as determined from analysis of high resolution s scans of model (A) two-component and (B) five-component externally mixed populations, from laboratory based (C) synthetic and (D) microcosm phytoplankton bloom experiments conducted in a MART, and (E) from underway measurements of nascent SSA generated by the sea-sweep during the WACS cruise in the Atlantic Ocean.

curve was fit to five summed sigmoidal curves that were centered at the anticipated s_{crit} values that corresponded to the predicted κ-values of each particle type (Figure 2B). The relative concentration of each particle type was then deduced from the height of each individual sigmoid, and the derived fractions agreed to within 10% of the experimental values. This serves as proof of concept that, although complex systems result in visibly broad activation curves for a continuum of particle types, activation curves generated from SR-CCN data sets can be considered within a framework that treats the overall activation curve as the linear combination of the activation of individual particle types (i.e., that have distinct κ-values) in an external aerosol mixture.

These bottom-up observations, along with the multicomponent activation framework, provide an experimental validation of the general idea that the slope of an activation curve when fit to a single sigmoid is related to the extent of chemical heterogeneity, with a wider sigmoid corresponding to greater chemical heterogeneity or more particle types.[31,35,47] For example, Cerully et al.[35] showed that the absolute value of the sigmoid slope was usually much larger for ambient aerosols than could be explained by the inherent width set by experimental factors, which they interpreted as an indication of the extent of external mixing. However, the use of a single sigmoid during fitting inherently assumes that there is a particular, continuous distribution in mixing state and therefore does not permit quantitative assessment of aerosol populations that display extreme heterogeneity, such as those shown in Figure 2, and that preclude fitting with a single sigmoid. The multicomponent activation framework has the ability to allow for more comprehensive examination of the particle mixing state compared to single-sigmoid methods, and also facilitates explicit determination of actual hygroscopicity distributions, as is developed further below.

3. HYGROSCOPICITY DIVERSITY OF SEA SPRAY AEROSOL PARTICLES

The bottom-up assessment and analysis methodology of the influence of particle mixing state on CCN activation curves developed above is extended and applied to the interpretation of activation curves for nascent SSA particles, which have been shown to exist as a complex, external mixture of varying particle types.[12,13] In one case, naturally more complex internal and external mixtures of SSA specifically were generated in the laboratory from synthetic and microcosm phytoplankton blooms in a manner analogous to wave breaking in the ocean using a Marine Aerosol Reference Tank (MART) (Figure S3 and Methods).[50] In a second case, nascent SSA particles were generated directly from the ocean surface using the NOAA PMEL sea-sweep[51] during the WACS I cruise in the Atlantic Ocean (Methods).[14] The observed activation curves for these systems have been interpreted using the concept of treating activation curves as a summation over individual sigmoids, as developed in section 2.3. However, one challenge in developing

DOI: 10.1021/acscentsci.5b00174
ACS Cent. Sci. 2015, 1, 132−141

a broadly applicable framework for external mixing is that it is best applied to SR-CCN data sets collected with high resolution in s, in which case explicit fitting of distinct sigmoids is possible (Figure 2B), but many data sets already exist that were collected with moderate to low s resolution. Further, the use of high s resolution requires longer overall scan times, which may not be amenable to all experiments.

We have therefore generalized the explicit multiple-sigmoid framework as a κ "basis-set" model in which the fraction of activated particles in a sample population can be deconstructed into prescribed hygroscopicity bins. This relaxes the need for the distinct steps in the activation curve, which are evident in the model five-component system, to be clearly observable for robust data fitting. In the general model, a range of κ-values is selected and divided logarithmically into bins, corresponding to s_{crit} bins of equal magnitude; for this study a κ range between 0.1 and 1.4 was used with six equivalent bins in s. The impact of κ bin resolution on our results is shown in Figure S4. These κ bins are converted to equivalent s_{crit} bins for the selected particle diameter. The observed normalized activation curves are integrated between sequential s_{crit} basis-set values (left-edge centered) to calculate the relative abundance of particles in each bin, resulting in a number-weighted κ distribution. The basis-set methodology extends beyond the general shape analysis of Su et al.[36] by generating an actual distribution of κ-values that characterizes the sample population. The basis-set methodology provides an explicit measure of mixing state diversity, in contrast to the traditional ensemble average κ-value calculated using the s_{crit} of the entire activation curve, which assumes that the population is internally mixed. The general features of the κ basis-set model permit extension of this analysis to any SR-CCN measurement, whether high or typical resolution, to determine κ distributions for samples ranging from simple model to complex ambient systems.

The basis-set model has been applied to SR-CCN measurements on the following marine-relevant systems: the laboratory generated (i) two- and (ii) five-component external mixtures discussed above; nascent SSA from (iii) synthetic and (iv) microcosm phytoplankton bloom experiments conducted in a MART;[50] and (v) nascent SSA generated from the surface ocean using the sea-sweep during the WACS I cruise in the Atlantic Ocean.[14] The synthetic bloom was produced from synthetic seawater after sequential addition of the five marine organic mimics in Table 1 (Figure S5). The transfer of organic species from the bulk water to aerosol phase during the synthetic bloom experiment was confirmed by measuring distributions (ranging from 0.1 to 0.3 organic volume fraction) of organic volume fractions by atomic force microscopy (AFM) for aerosol particles with diameters between 300 and 500 nm (Figure S6). The measurements for the microcosm bloom were performed at the beginning and end of the phytoplankton bloom life cycle for a bloom grown from ocean water collected off the Scripps Pier in La Jolla, CA; only the measurements made at the end are shown here, as no substantial difference was found between the measurements made at the beginning and end, indicating that biological productivity did not impact measured hygroscopicity distributions. The WACS sea-sweep measurements assessed here were made both within Georges Bank,[14] a location where the surface chlorophyll-a concentration was relatively high, indicating fairly biologically active waters, and within the oligotrophic Sargasso Sea, a location where the surface chlorophyll-a concentration was relatively low. As no substantial differences were found between the measurements at these two locations, only the Georges Bank results are shown here.

The resulting κ distributions are distinct for each system, highlighting the sensitivity of the κ basis-set method to the distribution of particle mixing state (Figure 3). When applied to the two-component and five-component systems, the expected κ distribution is generally recovered, although some edge effects are evident (Figure 3A,B) where multiple κ bins are populated for the same model component as a result of the finite κ bin width and activation curve integration. It is also important to note that, due to the variation in κ for different lots of sea salt, the "salt" κ bin appears at different values between model systems. The activation curves for both the synthetic and microcosm phytoplankton bloom experiments are relatively sharp, and the κ distributions are correspondingly relatively narrow (Figure 3C,D). This indicates a small degree of mixing state diversity for these dry 50 nm SSA and a particle population that was largely internally mixed with respect to hygroscopicity. The most probable κ-value was determined to be 0.6−0.9, which translates to an ε_{org} = 0.25−0.45, assuming that the organic component had a pure κ-value of 0.2. This range is slightly larger than the ε_{org} determined by AFM (median ∼0.2), although is likely explained by the AFM having characterized particles that were >50 nm, specifically 300−500 nm.

A much wider distribution of κ-values was observed for nascent SSA generated by the sea-sweep during the WACS I cruise (Figure 3E) compared to the synthetic and microcosm bloom experiments. This suggests that a wide variety of particle types were emitted during that experiment. The range of derived κ-values indicates that the nascent SSA had compositions ranging from purely sea salt to purely organic, providing a quantitative explanation for the observed breadth of the SR-CCN activation curves (Figure 3E). However, the suggested abundance of SSA with purely sea salt composition is potentially overestimated by the presence of doubly charged particles, which have been accounted for in the laboratory studies (excluding the five-component external mixture). The κ distribution peaks around κ = 0.50, suggesting that a substantial fraction of the nascent SSA particles had large organic fractions, with ε_{org} > 65%. Overall, application of the κ basis-set methodology to these various case studies demonstrates the potential for high-resolution SR-CCN measurements to be used in the determination of the distribution of κ-values, which is related to the particle mixing state diversity and goes beyond the typically reported effective κ, which may not actually represent the true system average nor characterize the actual behavior of the distribution within the atmosphere.

4. CCN IN MARINE ENVIRONMENTS AND BEYOND

The broader implications toward cloud droplet properties of considering atmospheric particulates as having unique distributions of particles with different chemical compositions (and therefore different hygroscopicities), as opposed to an internal mixture, are illustrated as a thought experiment in Figure 4. The particle−particle chemical diversity within a given air mass can be highly variable and is determined by the fundamental diversity in sources (such as those illustrated in Figure 3), chemical transformations of atmospheric particles, and mixing of different air masses.[52] This chemical diversity is represented here by using a variety of κ distributions of varying shape (Figure 4C). Using these distributions, the ratio between the number of particles that would activate at a given super-

DOI: 10.1021/acscentsci.5b00174
ACS Cent. Sci. 2015, 1, 132−141

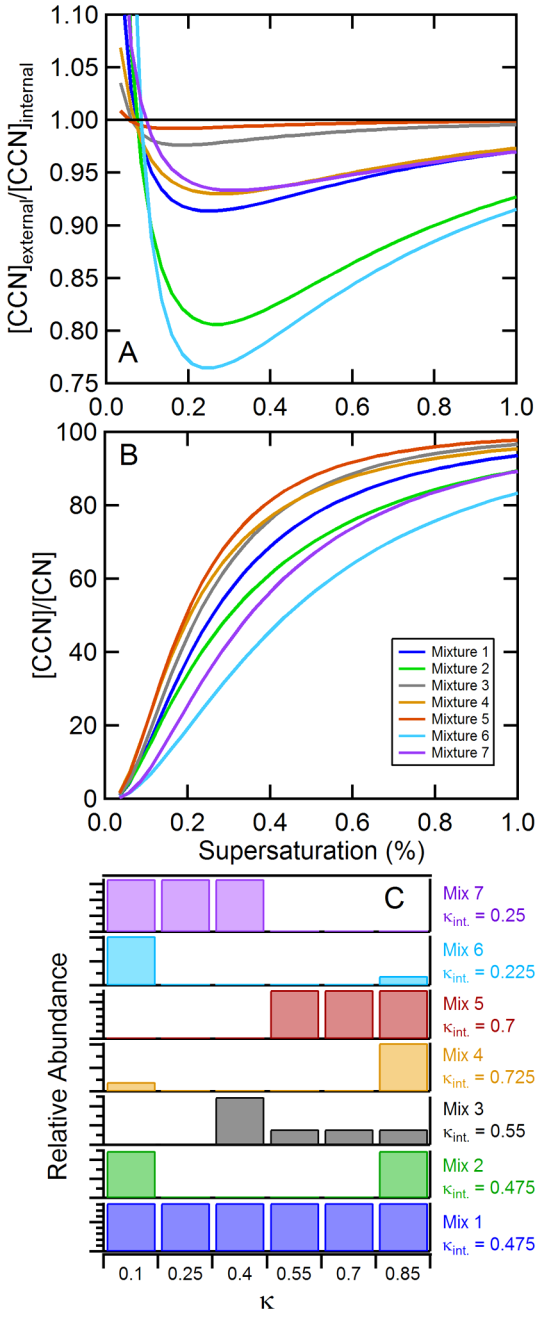

Figure 4. (A) The ratio between the number of particles activated (i.e., [CCN]) for an external mixture versus an internal mixture of particles and (B) the percent of particles activated for the external mixing case as a function of s for the κ distributions shown in panel C. The associated κ-value for each distribution, assuming internal mixing, is shown next to the distribution.

saturation for an external mixture versus an equivalent internal mixture (i.e., an internal mixture where the κ is calculated using volume mixing rules) has been calculated as $R_{CCN,E/I}(s) = [CCN]_{external}/[CCN]_{internal}$. The resulting $R_{CCN,E/I}$ values characterize the extent to which treating the particle population as an internal mixture leads to an under ($R_{CCN,E/I} < 1$) or over ($R_{CCN,E/I} > 1$) prediction in the actual fraction of CCN activated. A representative log-normal particle size distribution has been used (median D_p = 80 nm and σ_g = 1.7), and, although particle composition can be size dependent, each particle type (i.e., different κ) was assumed to have the same overall size distribution shape (Figure S7).

The importance of considering the particle mixing state explicitly depends on both the nature of the κ distribution and the supersaturation (Figure 4A). The $R_{CCN,E/I}$ exhibit a distinct minimum with s for all κ distributions, around s = 0.25% for the size distribution used here, and are lesser than unity at all but the smallest s (<0.1%). This indicates that an external mixing assumption will generally underestimate the extent of cloud drop activation. The $R_{CCN,E/I}$ at larger s asymptotically approach unity because, as s increases, an increasingly large fraction of the total particle number can activate (Figure 4B). The calculated minimum $R_{CCN,E/I}$ values range from close to 1 for relatively narrow κ distributions (e.g., mixture 5) to <0.85 for broad κ mixtures composed of particles with very different κ-values. The calculated minimum $R_{CCN,E/I}$ generally increases as the diversity of and difference between particle types increase with respect to their κ-values. The smallest $R_{CCN,E/I}$ values occur for mixtures in which there are only a few components having very different hygroscopicities. The results shown in Figure 4 are particular to the assumed size distribution, and the s at which the minimum in $R_{CCN,E/I}$ occurs is nominally linked to the overlap between the median D_p that characterizes the distribution and the s_{crit} vs size relationship for the internally mixed particles (Figure S8). Consequently, the position of the $R_{CCN,E/I}$ minimum increases if the median D_p were assumed smaller, and vice versa, and is more sensitive to shifts toward smaller sizes. However, shifts in the assumed D_p do not impact the minimum value of $R_{CCN,E/I}$ (Figure S9). The overall s dependence of $R_{CCN,E/I}$ indicates that proper accounting for mixing state will generally have a larger impact on cloud droplet properties in cloud systems where the maximum s remains below approximately 0.5%, such as those typically associated with stratocumulus clouds where typical values for s are around 0.2%.

5. CONCLUSIONS

A framework for the interpretation of CCN activation curves that accounts for diversity in individual particle hygroscopicity, which is driven by compositional diversity, has been introduced. The capabilities of this multicomponent framework were demonstrated using molecular mimics in which the activation of internally and externally mixed particle distributions of varying complexity was measured. The molecular mimics considered here were of particular relevance to marine environments in which SSA particles with a wide range of individual particle compositions are known to be generated. It was shown that, by considering a CCN activation curve as a sum of activation curves for individual particle types (i.e., particles with distinct compositions and hygroscopicities), the relative populations of these particle types can be retrieved. This represents an important advance over typical methods, which consider only the effective behavior and underplay the complicating influence of particle mixing state. The new framework was applied to the interpretation of laboratory and field observations of nascent SSA particles, which are complex mixtures of particle types with varying composition, to retrieve population-weighted distributions of κ hygroscopicity parameters. The importance of considering mixing state effects when interpreting the activation of such complex mixtures is apparent in the retrieved κ distributions, especially in the case of the field observations for which very broad distributions are obtained indicating that a wide diversity of particle types existed. Proper accounting for particle mixing state was shown to be important

DOI: 10.1021/acscentsci.5b00174
ACS Cent. Sci. 2015, 1, 132−141

to the assessment of the proper influence of particle composition, and more importantly compositional diversity, on clouds and global climate.

6. METHODS

Values of κ were measured for 50 nm dry diameter particles composed of single compounds or their internal and external aerosol mixtures using an SR-CCN method (Figure S1). The analysis can also be extended to particles with dry diameters other than 50 nm (Figure S10). Briefly, for each system the ratio between the total particle number concentration (CN) and the cloud active particle concentration (CCN) was measured as a function of supersaturation (s), from s between 0.1 and 1.0%, with $f_{CCN}(s) = [CCN]/[CN]$. The s_{crit} values for each given chemical system were determined either by visual inspection (five-component external mixture fit with one curve) or by fitting of a sigmoid to the observed activation curves (f_{CCN} versus s), from which effective κ-values were determined[5] (larger s_{crit} correspond to smaller κ at a given size). The SR-CCN measurements were made using high s resolution, up to four points per 0.1% s (see the Supporting Information). This is much higher resolution than is commonly used[14] and was found to provide more accurate constraints on the shape of the activation curve. The shapes of the activation curves and the associated s_{crit} and κ-values for the pure compounds and internal mixtures used in this study were highly dependent on the s resolution used, especially when there were few f_{CCN} measurements near the s_{crit}. The collection of high s resolution scans enables determination of well-constrained κ-values and very sharp SR-CCN activation curves.

Activation curves were measured for internal and external mixtures of varying chemical complexity that were generated using a few different methods (see the Supporting Information for more details). Simple internal mixtures (in which all particles have the same composition) of pure compounds and model multicomponent systems were generated by atomization or nebulization.

■ ASSOCIATED CONTENT

Supporting Information

The following file is available free of charge on the ACS Publications website at DOI: 10.1021/acscentsci.5b00174.

Further details on the aerosol generation methods used, the materials used, the size resolved cloud condensation nuclei (SR-CCN) method, the atomic force microscopy method, and the calculations described in section 4 (PDF)

■ AUTHOR INFORMATION

Corresponding Author

*E-mail: tbertram@chem.wisc.edu.

Funding

This work was funded by the National Science Foundation through the Center for Aerosol Impacts on Climate and the Environment under Grant No. CHE 1305427. P.K.Q. was supported by the National Oceanographic and Atmospheric Administration Climate Program Office. Any opinions, findings, and conclusions or recommendations expressed in this material are those of the authors and do not necessarily reflect the views of the National Science Foundation.

Notes

The authors declare no competing financial interest.

■ ACKNOWLEDGMENTS

The authors thank Olivia S. Ryder, Sara D. Forestieri, Nicole R. Campbell, and Professor Vicki H. Grassian, University of Iowa for helpful discussions. The authors thank M. Dale Stokes, Grant B. Deane, and the entire staff of the Scripps Institution of Oceanography Hydraulics Laboratory for helpful discussions pertaining to the sea spray aerosol production. This is PMEL contribution number 4325.

■ REFERENCES

(1) IPCC. *Climate Change 2013: The Physical Science Basis. Contribution of Working Group I to the Fifth Assessment Report of the Intergovernmental Panel on Climate Change*; Cambridge University Press: Cambridge, U.K., and New York, NY, USA, 2013; p 1535.

(2) Hegg, D. A.; Covert, D. S.; Jonsson, H. H.; Woods, R. K. A simple relationship between cloud drop number concentration and precursor aerosol concentration for the regions of Earth's large marine stratocumulus decks. *Atmos. Chem. Phys.* **2012**, *12*, 1229−1238.

(3) Bzdek, B. R.; Pennington, M. R.; Johnston, M. V. Single particle chemical analysis of ambient ultrafine aerosol: A review. *J. Aerosol Sci.* **2012**, *52*, 109−120.

(4) Farmer, D. K.; Cappa, C. D.; Kreidenweis, S. M. Atmospheric Processes and Their Controlling Influence on Cloud Condensation Nuclei Activity. *Chem. Rev.* **2015**, *115*, 4199−4217.

(5) Petters, M. D.; Kreidenweis, S. M. A single parameter representation of hygroscopic growth and cloud condensation nucleus activity. *Atmos. Chem. Phys.* **2007**, *7*, 1961−1971.

(6) Kreidenweis, S. M.; Asa-Awuku, A. Aerosol Hygroscopicity: Particle Water Content and Its Role in Atmospheric Processes. In *Treatise on Geochemistry*, 2nd ed.; Holland, H. D., Turekian, K. K., Eds.; Elsevier: Oxford, 2014; Vol. *5*, pp 331−361.

(7) Quinn, P. K.; Collins, D. B.; Grassian, V. H.; Prather, K. A.; Bates, T. S. Chemistry and Related Properties of Freshly Emitted Sea Spray Aerosol. *Chem. Rev.* **2015**, *115*, 4383−4399.

(8) O'Dowd, C. D.; De Leeuw, G. Marine aerosol production: a review of the current knowledge. *Philos. Trans. R. Soc., A* **2007**, *365*, 1753−1774.

(9) O'Dowd, C. D.; Facchini, M. C.; Cavalli, F.; Ceburnis, D.; Mircea, M.; Decesari, S.; Fuzzi, S.; Yoon, Y. J.; Putaud, J. P. Biogenically driven organic contribution to marine aerosol. *Nature* **2004**, *431*, 676−680.

(10) Facchini, M. C.; Rinaldi, M.; Decesari, S.; Carbone, C.; Finessi, E.; Mircea, M.; Fuzzi, S.; Ceburnis, D.; Flanagan, R.; Nilsson, E. D.; de Leeuw, G.; Martino, M.; Woeltjen, J.; O'Dowd, C. D. Primary submicron marine aerosol dominated by insoluble organic colloids and aggregates. *Geophys. Res. Lett.* **2008**, *35*, 5.

(11) Keene, W. C.; Maring, H.; Maben, J. R.; Kieber, D. J.; Pszenny, A. A. P.; Dahl, E. E.; Izaguirre, M. A.; Davis, A. J.; Long, M. S.; Zhou, X. L.; Smoydzin, L.; Sander, R. Chemical and physical characteristics of nascent aerosols produced by bursting bubbles at a model air-sea interface. *J. Geophys. Res.: Atmos.* **2007**, *112*, D21202.

(12) Prather, K. A.; Bertram, T. H.; Grassian, V. H.; Deane, G. B.; Stokes, M. D.; DeMott, P. J.; Aluwihare, L. I.; Palenik, B. P.; Azam, F.; Seinfeld, J. H.; Moffet, R. C.; Molina, M. J.; Cappa, C. D.; Geiger, F. M.; Roberts, G. C.; Russell, L. M.; Ault, A. P.; Baltrusaitis, J.; Collins, D. B.; Corrigan, C. E.; Cuadra-Rodriguez, L. A.; Ebben, C. J.; Forestieri, S. D.; Guasco, T. L.; Hersey, S. P.; Kim, M. J.; Lambert, W. F.; Modini, R. L.; Mui, W.; Pedler, B. E.; Ruppel, M. J.; Ryder, O. S.; Schoepp, N. G.; Sullivan, R. C.; Zhao, D. F. Bringing the ocean into the laboratory to probe the chemical complexity of sea spray aerosol. *Proc. Natl. Acad. Sci. U.S.A.* **2013**, *110*, 7550−7555.

(13) Ault, A. P.; Moffet, R. C.; Baltrusaitis, J.; Collins, D. B.; Ruppel, M. J.; Cuadra-Rodriguez, L. A.; Zhao, D. F.; Guasco, T. L.; Ebben, C. J.; Geiger, F. M.; Bertram, T. H.; Prather, K. A.; Grassian, V. H. Size-Dependent Changes in Sea Spray Aerosol Composition and Properties with Different Seawater Conditions. *Environ. Sci. Technol.* **2013**, *47*, 5603−5612.

(14) Quinn, P. K.; Bates, T. S.; Schulz, K. S.; Coffman, D. J.; Frossard, A. A.; Russell, L. M.; Keene, W. C.; Kieber, D. J.

DOI: 10.1021/acscentsci.5b00174
ACS Cent. Sci. 2015, 1, 132−141

Contribution of sea surface carbon pool to organic matter enrichment in sea spray aerosol. *Nat. Geosci.* **2014**, *7*, 228−232.
(15) Kaku, K. C.; Hegg, D. A.; Covert, D. S.; Santarpia, J. L.; Jonsson, H.; Buzorius, G.; Collins, D. R. Organics in the Northeastern Pacific and their impacts on aerosol hygroscopicity in the subsaturated and supersaturated regimes. *Atmos. Chem. Phys.* **2006**, *6*, 4101−4115.
(16) Ault, A. P.; Guasco, T. L.; Baltrusaitis, J.; Ryder, O. S.; Trueblood, J. V.; Collins, D. B.; Ruppel, M. J.; Cuadra-Rodriguez, L. A.; Prather, K. A.; Grassian, V. H. Heterogeneous Reactivity of Nitric Acid with Nascent Sea Spray Aerosol: Large Differences Observed between and within Individual Particles. *J. Phys. Chem. Lett.* **2014**, *5*, 2493−2500.
(17) Ault, A. P.; Guasco, T. L.; Ryder, O. S.; Baltrusaitis, J.; Cuadra-Rodriguez, L. A.; Collins, D. B.; Ruppel, M. J.; Bertram, T. H.; Prather, K. A.; Grassian, V. H. Inside versus Outside: Ion Redistribution in Nitric Acid Reacted Sea Spray Aerosol Particles as Determined by Single Particle Analysis. *J. Am. Chem. Soc.* **2013**, *135*, 14528−14531.
(18) Ault, A. P.; Zhao, D. F.; Ebben, C. J.; Tauber, M. J.; Geiger, F. M.; Prather, K. A.; Grassian, V. H. Raman microspectroscopy and vibrational sum frequency generation spectroscopy as probes of the bulk and surface compositions of size-resolved sea spray aerosol particles. *Phys. Chem. Chem. Phys.* **2013**, *15*, 6206−6214.
(19) Guasco, T. L.; Cuadra-Rodriguez, L. A.; Pedler, B. E.; Ault, A. P.; Collins, D. B.; Zhao, D. F.; Kim, M. J.; Ruppel, M. J.; Wilson, S. C.; Pomeroy, R. S.; Grassian, V. H.; Azam, F.; Bertram, T. H.; Prather, K. A. Transition Metal Associations with Primary Biological Particles in Sea Spray Aerosol Generated in a Wave Channel. *Environ. Sci. Technol.* **2014**, *48*, 1324−1333.
(20) Gunthe, S. S.; King, S. M.; Rose, D.; Chen, Q.; Roldin, P.; Farmer, D. K.; Jimenez, J. L.; Artaxo, P.; Andreae, M. O.; Martin, S. T.; Pöschl, U. Cloud condensation nuclei in pristine tropical rainforest air of Amazonia: size-resolved measurements and modeling of atmospheric aerosol composition and CCN activity. *Atmos. Chem. Phys.* **2009**, *9*, 7551−7575.
(21) Rose, D.; Gunthe, S. S.; Su, H.; Garland, R. M.; Yang, H.; Berghof, M.; Cheng, Y. F.; Wehner, B.; Achtert, P.; Nowak, A.; Wiedensohler, A.; Takegawa, N.; Kondo, Y.; Hu, M.; Zhang, Y.; Andreae, M. O.; Pöschl, U. Cloud condensation nuclei in polluted air and biomass burning smoke near the mega-city Guangzhou, China − Part 2: Size-resolved aerosol chemical composition, diurnal cycles, and externally mixed weakly CCN-active soot particles. *Atmos. Chem. Phys.* **2011**, *11*, 2817−2836.
(22) Meskhidze, N.; Xu, J.; Gantt, B.; Zhang, Y.; Nenes, A.; Ghan, S. J.; Liu, X.; Easter, R.; Zaveri, R. Global distribution and climate forcing of marine organic aerosol: 1. Model improvements and evaluation. *Atmos. Chem. Phys.* **2011**, *11*, 11689−11705.
(23) Westervelt, D. M.; Moore, R. H.; Nenes, A.; Adams, P. J. Effect of primary organic sea spray emissions on cloud condensation nuclei concentrations. *Atmos. Chem. Phys.* **2012**, *12*, 89−101.
(24) Cubison, M. J.; Ervens, B.; Feingold, G.; Docherty, K. S.; Ulbrich, I. M.; Shields, L.; Prather, K.; Hering, S.; Jimenez, J. L. The influence of chemical composition and mixing state of Los Angeles urban aerosol on CCN number and cloud properties. *Atmos. Chem. Phys.* **2008**, *8*, 5649−5667.
(25) Ervens, B.; Cubison, M.; Andrews, E.; Feingold, G.; Ogren, J. A.; Jimenez, J. L.; DeCarlo, P.; Nenes, A. Prediction of cloud condensation nucleus number concentration using measurements of aerosol size distributions and composition and light scattering enhancement due to humidity. *J. Geophys. Res.: Atmos.* **2007**, *112*, D10S32.
(26) Asa-Awuku, A.; Moore, R. H.; Nenes, A.; Bahreini, R.; Holloway, J. S.; Brock, C. A.; Middlebrook, A. M.; Ryerson, T. B.; Jimenez, J. L.; DeCarlo, P. F.; Hecobian, A.; Weber, R. J.; Stickel, R.; Tanner, D. J.; Huey, L. G. Airborne cloud condensation nuclei measurements during the 2006 Texas Air Quality Study. *J. Geophys. Res.: Atmos.* **2011**, *116*, D11201.
(27) Levin, E. J. T.; Prenni, A. J.; Palm, B. B.; Day, D. A.; Campuzano-Jost, P.; Winkler, P. M.; Kreidenweis, S. M.; DeMott, P. J.; Jimenez, J. L.; Smith, J. N. Size-resolved aerosol composition and its link to hygroscopicity at a forested site in Colorado. *Atmos. Chem. Phys.* **2014**, *14*, 2657−2667.
(28) Lance, S.; Nenes, A.; Mazzoleni, C.; Dubey, M. K.; Gates, H.; Varutbangkul, V.; Rissman, T. A.; Murphy, S. M.; Sorooshian, A.; Flagan, R. C.; Seinfeld, J. H.; Feingold, G.; Jonsson, H. H. Cloud condensation nuclei activity, closure, and droplet growth kinetics of Houston aerosol during the Gulf of Mexico Atmospheric Composition and Climate Study (GoMACCS). *J. Geophys. Res.: Atmos.* **2009**, *114*, D00F15.
(29) Broekhuizen, K.; Chang, R. Y. W.; Leaitch, W. R.; Li, S. M.; Abbatt, J. P. D. Closure between measured and modeled cloud condensation nuclei (CCN) using size-resolved aerosol compositions in downtown Toronto. *Atmos. Chem. Phys.* **2006**, *6*, 2513−2524.
(30) Medina, J.; Nenes, A.; Sotiropoulou, R. E. P.; Cottrell, L. D.; Ziemba, L. D.; Beckman, P. J.; Griffin, R. J. Cloud condensation nuclei closure during the International Consortium for Atmospheric Research on Transport and Transformation 2004 campaign: Effects of size-resolved composition. *J. Geophys. Res.: Atmos.* **2007**, *112*, D10S31.
(31) Padró, L. T.; Moore, R. H.; Zhang, X.; Rastogi, N.; Weber, R. J.; Nenes, A. Mixing state and compositional effects on CCN activity and droplet growth kinetics of size-resolved CCN in an urban environment. *Atmos. Chem. Phys.* **2012**, *12*, 10239−10255.
(32) Collins, D. B.; Ault, A. P.; Moffet, R. C.; Ruppel, M. J.; Cuadra-Rodriguez, L. A.; Guasco, T. L.; Corrigan, C. E.; Pedler, B. E.; Azam, F.; Aluwihare, L. I.; Bertram, T. H.; Roberts, G. C.; Grassian, V. H.; Prather, K. A. Impact of marine biogeochemistry on the chemical mixing state and cloud forming ability of nascent sea spray aerosol. *J. Geophys. Res.: Atmos.* **2013**, *118*, 8553−8565.
(33) Swietlicki, E.; Hansson, H. C.; Hameri, K.; Svenningsson, B.; Massling, A.; McFiggans, G.; McMurry, P. H.; Petaja, T.; Tunved, P.; Gysel, M.; Topping, D.; Weingartner, E.; Baltensperger, U.; Rissler, J.; Wiedensohler, A.; Kulmala, M. Hygroscopic properties of submicrometer atmospheric aerosol particles measured with H-TDMA instruments in various environments - a review. *Tellus, Ser. B* **2008**, *60*, 432−469.
(34) Wex, H.; McFiggans, G.; Henning, S.; Stratmann, F., Influence of the external mixing state of atmospheric aerosol on derived CCN number concentrations. *Geophys. Res. Lett.* **2010**, *37*.
(35) Cerully, K. M.; Raatikainen, T.; Lance, S.; Tkacik, D.; Tiitta, P.; Petaja, T.; Ehn, M.; Kulmala, M.; Worsnop, D. R.; Laaksonen, A.; Smith, J. N.; Nenes, A. Aerosol hygroscopicity and CCN activation kinetics in a boreal forest environment during the 2007 EUCAARI campaign. *Atmos. Chem. Phys.* **2011**, *11*, 12369−12386.
(36) Su, H.; Rose, D.; Cheng, Y. F.; Gunthe, S. S.; Massling, A.; Stock, M.; Wiedensohler, A.; Andreae, M. O.; Poschl, U. Hygroscopicity distribution concept for measurement data analysis and modeling of aerosol particle mixing state with regard to hygroscopic growth and CCN activation. *Atmos. Chem. Phys.* **2010**, *10*, 7489−7503.
(37) Burrows, S. M.; Ogunro, O.; Frossard, A. A.; Russell, L. M.; Rasch, P. J.; Elliott, S. M. A physically based framework for modeling the organic fractionation of sea spray aerosol from bubble film Langmuir equilibria. *Atmos. Chem. Phys.* **2014**, *14*, 13601−13629.
(38) Long, M. S.; Keene, W. C.; Kieber, D. J.; Erickson, D. J.; Maring, H. A sea-state based source function for size- and composition-resolved marine aerosol production. *Atmos. Chem. Phys.* **2011**, *11*, 1203−1216.
(39) Hansell, D. A. Recalcitrant Dissolved Organic Carbon Fractions. *Annu. Rev. Mar. Sci.* **2013**, *5*, 421−445.
(40) Corrigan, C. E.; Novakov, T. Cloud condensation nucleus activity of organic compounds: a laboratory study. *Atmos. Environ.* **1999**, *33*, 2661−2668.
(41) Hartz, K. E. H.; Tischuk, J. E.; Chan, M. N.; Chan, C. K.; Donahue, N. M.; Pandis, S. N. Cloud condensation nuclei activation of limited solubility organic aerosol. *Atmos. Environ.* **2006**, *40*, 605−617.
(42) Hori, M.; Ohta, S.; Murao, N.; Yamagata, S. Activation capability of water soluble organic substances as CCN. *J. Aerosol Sci.* **2003**, *34*, 419−448.

DOI: 10.1021/acscentsci.5b00174
ACS Cent. Sci. 2015, 1, 132−141

(43) Lu, J. W.; Rickards, A. M. J.; Walker, J. S.; Knox, K. J.; Miles, R. E. H.; Reid, J. P.; Signorell, R. Timescales of water transport in viscous aerosol: measurements on sub-micron particles and dependence on conditioning history. *Phys. Chem. Chem. Phys.* **2014**, *16*, 9819−9830.
(44) Ruehl, C. R.; Chuang, P. Y.; Nenes, A.; Cappa, C. D.; Kolesar, K. R.; Goldstein, A. H. Strong evidence of surface tension reduction in microscopic aqueous droplets. *Geophys. Res. Lett.* **2012**, *39*, L23801.
(45) Ruehl, C. R.; Wilson, K. R. Surface Organic Mono layers Control the Hygroscopic Growth of Submicrometer Particles at High Relative Humidity. *J. Phys. Chem. A* **2014**, *118*, 3952−3966.
(46) Haynes, W. M.; Lide, D. R. *CRC handbook of chemistry and physics: a ready-reference book of chemical and physical data*, 95th ed.; CRC Press: Boca Raton, FL, 2014.
(47) Bougiatioti, A.; Nenes, A.; Fountoukis, C.; Kalivitis, N.; Pandis, S. N.; Mihalopoulos, N. Size-resolved CCN distributions and activation kinetics of aged continental and marine aerosol. *Atmos. Chem. Phys.* **2011**, *11*, 8791−8808.
(48) Leck, C.; Bigg, E. K. Source and evolution of the marine aerosol - A new perspective. *Geophys. Res. Lett.* **2005**, *32*, L19803.
(49) Rose, D.; Gunthe, S. S.; Mikhailov, E.; Frank, G. P.; Dusek, U.; Andreae, M. O.; Poschl, U. Calibration and measurement uncertainties of a continuous-flow cloud condensation nuclei counter (DMT-CCNC): CCN activation of ammonium sulfate and sodium chloride aerosol particles in theory and experiment. *Atmos Chem. Phys.* **2008**, *8*, 1153−1179.
(50) Stokes, M. D.; Deane, G. B.; Prather, K.; Bertram, T. H.; Ruppel, M. J.; Ryder, O. S.; Brady, J. M.; Zhao, D. A Marine Aerosol Reference Tank system as a breaking wave analogue for the production of foam and sea-spray aerosols. *Atmos. Meas. Technol.* **2013**, *6*, 1085−1094.
(51) Bates, T. S.; Quinn, P. K.; Frossard, A. A.; Russell, L. M.; Hakala, J.; Petäjä, T.; Kulmala, M.; Covert, D. S.; Cappa, C. D.; Li, S. M.; Hayden, K. L.; Nuaaman, I.; McLaren, R.; Massoli, P.; Canagaratna, M. R.; Onasch, T. B.; Sueper, D.; Worsnop, D. R.; Keene, W. C. Measurements of ocean derived aerosol off the coast of California. *J. Geophys. Res.: Atmos.* **2012**, *117*, D00V15.
(52) Fierce, L.; Riemer, N.; Bond, T. C. When is cloud condensation nuclei activity sensitive to particle characteristics at emission? *J. Geophys. Res.: Atmos.* **2013**, *118*, 13476−13488.

DOI: 10.1021/acscentsci.5b00174
ACS Cent. Sci. 2015, 1, 132−141